Design and Real-time Implementation of Perturbation Observer based Sliding-mode Control for VSC-HVDC Systems

B. Yang[a,b], Y. Y. Sang[b], K. Shi[b], Wei Yao[c], L. Jiang[b,*], T. Yu[d]

[a] *Faculty of Electric Power Engineering, Kunming University of Science and Technology, Kunming, 650504, China*
[b] *Department of Electrical Engineering and Electronics, University of Liverpool, Liverpool, L69 3GJ, United Kingdom*
[c] *State Key Laboratory of Advanced Electromagnetic Engineering and Technology, Huazhong University of Science and Technology, Wuhan, 430074, China*
[d] *School of Electrical Engineering, South China University of Technology, Guangzhou, Guangdong, 510641, China*

Abstract

This paper develops a perturbation observer based sliding-mode control (POSMC) scheme for voltage source converter based high voltage direct current (VSC-HVDC) systems. The combinatorial effect of nonlinearities, parameter uncertainties, unmodelled dynamics and time-varying external disturbances is aggregated into a perturbation, which is estimated online by a sliding-mode state and perturbation observer. POSMC does not require an accurate system model and only one state measurement is needed. Moreover, a significant robustness can be provided through the real-time compensation of the per-

*Corresponding author
Email address: ljiang@liverpool.ac.uk (L. Jiang)

turbation. Four case studies are carried out on the VSC-HVDC system, such as active and reactive power tracking, AC bus fault, system parameter uncertainties, and weak AC gird connection. Simulation results verify its advantages over vector control and feedback linearization sliding-mode control. Then a hardware-in-the-loop (HIL) test is undertaken to validate the implementation feasibility of the proposed approach.
Keywords: sliding-mode control, perturbation observer, VSC-HVDC systems, HIL test

---

1. Introduction

Voltage source converter based high voltage direct current (VSC-HVDC) systems using insulated gate bipolar transistor (IGBT) technology have attracted increasing attentions due to the interconnection between the mainland and offshore wind farms, power flow regulation in alternating current (AC) power systems, long distance transmission (Flourentzou, Agelidis and Demetriades, 2009), and introduction of the supergrid, which is a large-scale power grid interconnected between national power grids (Hertema and Ghandhari, 2010). The main feature of the VSC-HVDC system is that no external voltage source is needed for communication, while active and reactive power at each AC grid can be independently controlled (Zhang, 2011).

Traditionally, control of the VSC-HVDC system utilizes a nested-loop d-q vector control (VC) approach based on linear proportional-integral (PI) methods (Haileselassie, Molinas and Undeland, 2008), whose control performance may be degraded with the change of operation conditions as its control parameters are tuned from one-point linearization model (Li, Haskew and Xu, 2010). As VSC-HVDC systems are highly nonlinear resulting from converters and also operate in power systems with modelling uncertainties, many advanced control approaches are developed to provide a consistent control performance under various operation conditions, such as feedback linearization control (FLC) (Ruan, Li, Peng, Sun and Lie, 2007), which fully compensated the nonlinearities with the requirement of an accurate system model. Linear matrix inequality (LMI)-based robust control was developed in (Durrant, Werner and Abbott, 2004) to maximize the size of the uncertainty region within which closed loop stability is maintained. In addition, adaptive backstepping control was designed to estimate the uncertain parameters by (Ruan, Li, Jiao, Sun and Lie, 2007). In (Zhang, Harnefors and Nee, 2011), power-synchronization control was employed to greatly increase the short-circuit capacity to the AC system. However, the aforementioned methods may not be adequate to simultaneously handle perturbations such as modelling uncertainties and time-varying external disturbances .

Based on the variable structure control strategy, sliding-mode control (SMC) is an effective and high-frequency switching control for nonlinear systems with modelling uncertainties and time-varying external disturbances. The main idea of SMC is to maintain the system sliding on a surface in the state space via an appropriate switching logic, it features the simple implementation, disturbance rejection, fast response and strong robustness (Lordelo and Fazzolari, 2014). While the malignant effect of chattering phenomenon can be reduced by predictive variable structure (Huo, 2008) and self-tuning sliding mode (Zong, Zhao and Zhang, 2010), SMC has been applied on electrical vehicles (Gokasan, Bogosyan and Goering, 2006), power converters (Kessal and Rahmani, 2014), induction machines (Lascu, Boldea and Blaabjerg, 2004), wind turbines (Beltran, Ahmed-Ali and Benbouzid, 2008), ect. Moreover, a feedback linearization sliding-mode control (FLSMC) has been developed for the VSC-HVDC system to offer invariant stability to modelling uncertainties by (Moharana and Dash, 2010). Basically, SMC assumes perturbations to be bounded and the prior knowledge of these upper bounds is required. However, it may be difficult or sometimes impossible to obtain these upper bounds, thus the supreme upper bound is chosen to cover the whole range of perturbations. As a consequence, SMC based on this knowledge becomes over-conservative which may cause a poor tracking performance and undesirable control oscillations (Edwards and Spurgeon, 1998).

During the past decades, several elegant approaches based on observers have been proposed to estimate perturbations, including the unknown input observer (UIO) (Johnson, 1971), the disturbance observer (DOB) (Chen, Ballance, Gawthrop and O'Reilly, 2000), the equivalent input disturbance (EID) based estimation (She, Fang, Ohyama, Hashimoto and Wu, 2008), enhanced decentralized PI control via advanced disturbance observer (Sun, Li and Lee, 2015), the extended state observer (ESO) based active disturbance rejection control (ADRC) (Han, 2009), and practical multivariable control based on inverted decoupling and decentralized ADRC (Sun, Dong, Li and Lee, 2016). Among the above listed approaches, ESO requires the least amount of system information, in fact, only the system order needs to be known (Guo and Zhao, 2011). Due to such promising features, ESO based control schemes have become more and more popular. Recently, ESO based SMC has been developed to remedy the over-conservativeness of SMC via an online perturbation estimation. It observes both system states and perturbations by defining an extended state to represent the lumped perturbation, which can be then compensated online to improve the performance of system. Related applications can be referred to mechanical systems (Kwon and Chung, 2004), missile systems (Xia, Zhu and Fu, 2011), spherical robots (Yue, Liu, An and Sun, 2014), and DC-DC buck power converters (Wang, Li, Yang, Wu and Li, 2015).

This paper uses an ESO called sliding-mode state and perturbation observer (SMSPO) (Jiang, Wu and Wen, 2002; Liu, Wu, Zhou and Jiang, 2014) to estimate the combinatorial effect of nonlinearities, parameter uncertainties, unmodelled dynamics and time-varying external disturbances existed in VSC-HVDC systems, which is then compensated by the perturbation observer based sliding-mode control (POSMC). The motivation to use POSMC in this paper rather than SMC and our previous work (Jiang, Wu and Wen, 2002; Liu, Wu, Zhou and Jiang, 2014; Yang, Jiang, Yao and Wu, 2015) can be summarized as follows:

- The robustness of POSMC to the perturbation mostly depends on the perturbation compensation while the ground of the robustness in SMC (Gokasan, Bogosyan and Goering, 2006; Kessal and Rahmani, 2014; Lascu, Boldea and Blaabjerg, 2004; Beltran, Ahmed-Ali and Benbouzid, 2008; Moharana and Dash, 2010) is the discrete switching input. Furthermore, the upper bound of perturbation is replaced by the smaller bound of its estimation error, thus an over conservative control input is avoided and the tracking accuracy is improved.

- POSMC can provide greater robustness than that of nonlinear adaptive control (NAC) (Jiang, Wu and Wen, 2002; Liu, Wu, Zhou and Jiang, 2014) and perturbation observer based adaptive passive control (POAPC) (Yang, Jiang, Yao and Wu, 2015) due to its inherent property of disturbance rejection.

Compared to VC (Li, Haskew and Xu, 2010), POSMC can provide a consistent control performance under various operation condition of the VSC-HVDC system and improve the power tracking by eliminating the power overshoot. Compared to FLSMC (Moharana and Dash, 2010), POSMC only requires the measurement of active and reactive power and DC voltage, which can provide a significant robustness and avoid an over-conservative control input as the real perturbation is estimated and compensated online. Four case studies are carried out to evaluate the control performance of POSMC through simulation, such as active and reactive power tracking, AC bus fault, system parameter uncertainties and weak AC gird connection. Compared to the author's previous work on SMSPO (Jiang, Wu and Wen, 2002; Liu, Wu, Zhou and Jiang, 2014), a dSPACE simulator based hardware-in-the-loop (HIL) test is undertaken to validate its implementation feasibility.

The rest of the paper is organized as follows. In Section 2, the model of the two-terminal VSC-HVDC system is presented. In Section 3, POSMC design for the VSC-HVDC system is developed and discussed. Section 4 and 5 present the simulation and HIL results, respectively. Finally, conclusions are drawn in Section 6.

2. VSC-HVDC System Modelling

There are two VSCs in the VSC-HVDC system shown in Fig. 1, in which the rectifier regulates the DC voltage and reactive power, while the inverter regulates the active and reactive power. Only the balanced condition is considered, e.g., the three phases have identical parameters and their voltages and currents have the same amplitude while each phase shifts 120° between themselves. The rectifier dynamics can be written at the angular frequency

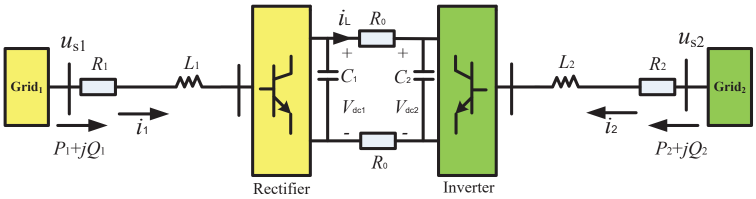

Figure 1: A standard two-terminal VSC-HVDC system

ω as (Ruan, Li, Jiao, Sun and Lie, 2007)

$$\begin{cases} \frac{\mathrm{d}i_{\mathrm{d1}}}{\mathrm{d}t} = -\frac{R_1}{L_1}i_{\mathrm{d1}} + \omega i_{\mathrm{q1}} + u_{\mathrm{d1}} \\ \frac{\mathrm{d}i_{\mathrm{q1}}}{\mathrm{d}t} = -\frac{R_1}{L_1}i_{\mathrm{q1}} - \omega i_{\mathrm{d1}} + u_{\mathrm{q1}} \\ \frac{\mathrm{d}V_{\mathrm{dc1}}}{\mathrm{d}t} = \frac{3u_{\mathrm{sq1}}i_{\mathrm{q1}}}{2C_1V_{\mathrm{dc1}}} - \frac{i_{\mathrm{L}}}{C_1} \end{cases} \tag{1}$$

where the rectifier is connected with the AC grid via the equivalent resistance and inductance R_1 and L_1, respectively. C_1 is the DC bus capacitor, $u_{\mathrm{d1}} = \frac{u_{\mathrm{sd1}} - u_{\mathrm{rd}}}{L_1}$ and $u_{\mathrm{q1}} = \frac{u_{\mathrm{sq1}} - u_{\mathrm{rq}}}{L_1}$.

The inverter dynamics is written as

$$\begin{cases} \frac{\mathrm{d}i_{\mathrm{d2}}}{\mathrm{d}t} = -\frac{R_2}{L_2}i_{\mathrm{d2}} + \omega i_{\mathrm{q2}} + u_{\mathrm{d2}} \\ \frac{\mathrm{d}i_{\mathrm{q2}}}{\mathrm{d}t} = -\frac{R_2}{L_2}i_{\mathrm{q2}} - \omega i_{\mathrm{d2}} + u_{\mathrm{q2}} \\ \frac{\mathrm{d}V_{\mathrm{dc2}}}{\mathrm{d}t} = \frac{3u_{\mathrm{sq2}}i_{\mathrm{q2}}}{2C_2V_{\mathrm{dc2}}} + \frac{i_{\mathrm{L}}}{C_2} \end{cases} \tag{2}$$

where the inverter is connected with the AC grid via the equivalent resistance and inductance R_2 and L_2, respectively. C_2 is the DC bus capacitor, $u_{\mathrm{d2}} =$

$\frac{u_{\mathrm{sd2}}-u_{\mathrm{id}}}{L_2}$ and $u_{\mathrm{q2}} = \frac{u_{\mathrm{sq2}}-u_{\mathrm{iq}}}{L_2}$.

The interconnection between the rectifier and inverter through DC cable is given as

$$V_{\mathrm{dc1}} i_{\mathrm{L}} = V_{\mathrm{dc2}} i_{\mathrm{L}} + 2R_0 i_{\mathrm{L}}^2 \tag{3}$$

where R_0 represents the equivalent DC cable resistance.

The phase-locked loop (PLL) (Jovcic, 2003) is used during the transformation of the *abc* frame to the *dq* frame. In the synchronous frame, u_{sd1}, u_{sd2}, u_{sq1}, and u_{sq2} are the d, q axes components of the respective AC grid voltages; i_{d1}, i_{d2}, i_{q1}, and i_{q2} are that of the line currents; u_{rd}, u_{id}, u_{rq}, and u_{iq} are that of the converter input voltages. P_1, P_2, Q_1, and Q_2 are the active and reactive powers transmitted from the AC grid to the VSC; V_{dc1} and V_{dc2} are the DC voltages; and i_{L} is the DC cable current.

At the rectifier side, the q-axis is set to be in phase with the AC grid voltage u_{s1}. Correspondingly, the q-axis is set to be in phase of the AC grid voltage u_{s2} at the inverter side. Hence, u_{sd1} and u_{sd2} are equal to 0 while u_{sq1} and u_{sq2} are equal to the magnitude of u_{s1} and u_{s2}. Note that this paper adopts such framework from (Moharana and Dash, 2010; Ruan, Li, Jiao, Sun and Lie, 2007; Ruan, Li, Peng, Sun and Lie, 2007) to provide a consistent control design procedure and an easy control performance comparison, other framework can also be used as shown in (Li, Haskew and Xu, 2010; Zhang, Harnefors and Nee, 2011). The only difference of these two alternatives is the derived system equations, while the control design is totally the same. In addition, it is assumed that the VSC-HVDC system is connected to sufficiently strong AC grids, such that the AC grid voltage remains as an ideal constant. The power flows from the AC grid can be given as

$$\begin{cases} P_1 = \frac{3}{2}\left(u_{\mathrm{sq1}}i_{\mathrm{q1}} + u_{\mathrm{sd1}}i_{\mathrm{d1}}\right) = \frac{3}{2}u_{\mathrm{sq1}}i_{\mathrm{q1}} \\ Q_1 = \frac{3}{2}\left(u_{\mathrm{sq1}}i_{\mathrm{d1}} - u_{\mathrm{sd1}}i_{\mathrm{q1}}\right) = \frac{3}{2}u_{\mathrm{sq1}}i_{\mathrm{d1}} \\ P_2 = \frac{3}{2}\left(u_{\mathrm{sq2}}i_{\mathrm{q2}} + u_{\mathrm{sd2}}i_{\mathrm{d2}}\right) = \frac{3}{2}u_{\mathrm{sq2}}i_{\mathrm{q2}} \\ Q_2 = \frac{3}{2}\left(u_{\mathrm{sq2}}i_{\mathrm{d2}} - u_{\mathrm{sd2}}i_{\mathrm{q2}}\right) = \frac{3}{2}u_{\mathrm{sq2}}i_{\mathrm{d2}} \end{cases} \tag{4}$$

3. POSMC Design for the VSC-HVDC System

3.1. Perturbation observer based sliding-mode control

Consider an uncertain nonlinear system which has the following canonical form

$$\begin{cases} \dot{x} = Ax + B(a(x) + b(x)u + d(t)) \\ y = x_1 \end{cases} \tag{5}$$

where $x = [x_1, x_2, \cdots, x_n]^{\mathrm{T}} \in \mathbb{R}^n$ is the state variable vector, $u \in \mathbb{R}$ and $y \in \mathbb{R}$ are the control input and system output, respectively. $a(x) : \mathbb{R}^n \mapsto \mathbb{R}$ and $b(x) : \mathbb{R}^n \mapsto \mathbb{R}$ are unknown smooth functions, and $d(t) : \mathbb{R}^+ \mapsto \mathbb{R}$ represents the time-varying external disturbance. The $n \times n$ matrix A and the $n \times 1$ matrix B are of the canonical form as follows

$$A = \begin{bmatrix} 0 & 1 & 0 & \cdots & 0 \\ 0 & 0 & 1 & \cdots & 0 \\ \vdots & & & & \vdots \\ 0 & 0 & 0 & \cdots & 1 \\ 0 & 0 & 0 & \cdots & 0 \end{bmatrix}_{n\times n}, \quad B = \begin{bmatrix} 0 \\ 0 \\ \vdots \\ 0 \\ 1 \end{bmatrix}_{n\times 1}$$

The perturbation of system (5) is defined as (Jiang, Wu and Wen, 2002; Liu, Wu, Zhou and Jiang, 2014; Yang, Jiang, Yao and Wu, 2015)

$$\Psi(x, u, t) = a(x) + (b(x) - b_0)u + d(t) \tag{6}$$

From the original system (5), the last state x_n can be rewritten in the presence of perturbation (6) as follows

$$\dot{x}_n = a(x) + (b(x) - b_0)u + d(t) + b_0 u = \Psi(x, u, t) + b_0 u \tag{7}$$

Define a *fictitious state* $x_{n+1} = \Psi(x, u, t)$. Then, system (5) can be extended as

$$\begin{cases} y = x_1 \\ \dot{x}_1 = x_2 \\ \vdots \\ \dot{x}_n = x_{n+1} + b_0 u \\ \dot{x}_{n+1} = \dot{\Psi}(\cdot) \end{cases} \tag{8}$$

The new state vector becomes $x_{\mathrm{e}} = [x_1, x_2, \cdots, x_n, x_{n+1}]^{\mathrm{T}}$, and following assumptions are made (Jiang, Wu and Wen, 2002)

- A.1 b_0 is chosen to satisfy: $|b(x)/b_0 - 1| \leq \theta < 1$, where θ is a positive constant.
- A.2 The functions $\Psi(x, u, t) : \mathbb{R}^n \times \mathbb{R} \times \mathbb{R}^+ \mapsto \mathbb{R}$ and $\dot{\Psi}(x, u, t) : \mathbb{R}^n \times \mathbb{R} \times \mathbb{R}^+ \mapsto \mathbb{R}$ are bounded over the domain of interest: $|\Psi(x, u, t)| \leq \gamma_1$, $|\dot{\Psi}(x, u, t)| \leq \gamma_2$ with $\Psi(0, 0, 0) = 0$ and $\dot{\Psi}(0, 0, 0) = 0$, where γ_1 and γ_2

are positive constants.

- A.3 The desired trajectory y_d and its up to nth-order derivative are continuous and bounded.

The above three assumptions ensure the effectiveness of such perturbation estimation based approach. In particular, assumptions A.1 and A.2 guarantee the closed-loop system stability with perturbation estimation, while assumption A.3 ensures POSMC can drive the system state x to track a desired state $x_\mathrm{d} = [y_\mathrm{d}, y_\mathrm{d}^{(1)}, \cdots, y_\mathrm{d}^{(n-1)}]^\mathrm{T}$ (Jiang, 2001). In the consideration of the worst case, e.g., $y = x_1$ is the only measurable state, an $(n{+}1)$th-order SMSPO (Jiang, Wu and Wen, 2002; Liu, Wu, Zhou and Jiang, 2014) for the extended system (8) is designed to estimate the system states and perturbation, shown as follows

$$\begin{cases} \dot{\hat{x}}_1 = \hat{x}_2 + \alpha_1 \tilde{x}_1 + k_1 \mathrm{sat}(\tilde{x}_1) \\ \qquad \vdots \\ \dot{\hat{x}}_n = \hat{\Psi}(\cdot) + \alpha_n \tilde{x}_1 + k_n \mathrm{sat}(\tilde{x}_1) + b_0 u \\ \dot{\hat{\Psi}}(\cdot) = \alpha_{n+1} \tilde{x}_1 + k_{n+1} \mathrm{sat}(\tilde{x}_1) \end{cases} \tag{9}$$

where $\tilde{x}_1 = x_1 - \hat{x}_1$, k_i and α_i, $i = 1, 2, \cdots, n+1$, are positive coefficients, function $\mathrm{sat}(\tilde{x}_1)$ is defined as $\mathrm{sat}(\tilde{x}_1) = \tilde{x}_1/|\tilde{x}_1|$ when $|\tilde{x}_1| > \epsilon$ and $\mathrm{sat}(\tilde{x}_1) = \tilde{x}_1/\epsilon$ when $|\tilde{x}_1| \leq \epsilon$. The effect and setting of the SMSPO parameters are provided as follows:

- **The Luenberger observer constants** α_i. Which are chosen to place the observer poles at the desired locations in the open left-half complex plane. In other words, α_i are chosen such that the root of $s^{n+1} + \alpha_1 s^n + \alpha_2 s^{n-1} + \cdots + \alpha_{n+1} = (s + \lambda_\alpha)^{n+1} = 0$ is in the open left-half complex plane. A larger value of α_i will accelerate the estimation rate of SMSPO but also result in a more significant effect of peaking phenomenon. Thus a trade-off between the estimation rate and effect of peaking phenomenon must be made through trial-and-error. Normally they are set to be much larger than the root of the closed-loop system to ensure a fast online estimation (Yang, Jiang, Yao and Wu, 2015).

- **The sliding surface constants** k_i**.** $k_1 \geq |\tilde{x}_2|_{\max}$ must be chosen to guarantee the estimation error of SMSPO (9) will enter into the sliding surface $S_{\mathrm{spo}}(\tilde{x}) = \tilde{x}_1 = 0$ at $t > t_{\mathrm{s}}$ and thereafter remain $S_{\mathrm{spo}} = 0$, $t \geq t_{\mathrm{s}}$(Jiang, 2001; Jiang, Wu and Wen, 2002). While the poles of the sliding surface λ_k are determined by choosing the ratio $k_i/k_1(i = 2, 3, \cdots, n+$

1) to put the root of $p^n+(k_2/k_1)p^{n-1}+\cdots+(k_n/k_1)p+(k_{n+1}/k_1) = (p+\lambda_k)^n = 0$ to be in the open left-half complex plane. Under Assumption A.2, SMSPO converges to a neighbourhood of the origin if gains k_i are properly selected, which has been proved in (Jiang, Wu and Wen, 2002; Hernandez and Barbot, 1996). For a given k_1, a larger k_i will accelerate the estimation rate of SMSPO but also result in a degraded observer stability. Thus a trade-off between the estimation rate and observer stability must be made through trial-and-error (Jiang, 2001).

- **The layer thickness constant of saturation function ϵ.** Which is a positive small scaler to replace the sign function by the saturation function, such that the chattering effect can be reduced. A larger ϵ will result in a smoother chattering but a larger steady-state estimation error. Consequently, a trade-off between the chattering effect and steady-state estimation error must be made through trial-and-error. In practice, a value closes to 0 is recommended.

Remark 1. When SMSPO is used to estimate the perturbation, the upper bound of the derivative of perturbation γ_2 is required to guarantee the estimation accuracy, and such upper bound will result in a conservative observer gain. However, the conservative gain is only included in the observer loop, not in the controller loop.

Define an estimated sliding surface as

$$\hat{S}(x,t) = \sum_{i=1}^{n} \rho_i(\hat{x}_i - y_{\mathrm{d}}^{(i-1)}) \tag{10}$$

where the estimated sliding surface gains $\rho_i = C_{n-1}^{i-1}\lambda_{\mathrm{c}}^{n-i}$, $i = 1, \cdots, n$, place all poles of the estimated sliding surface at $-\lambda_{\mathrm{c}}$, where $\lambda_{\mathrm{c}} > 0$.

The POSMC for system (5) is designed as

$$u = \frac{1}{b_0}\left[y_{\mathrm{d}}^{(n)} - \sum_{i=1}^{n-1} \rho_i(\hat{x}_{i+1} - y_{\mathrm{d}}^{(i)}) - \zeta\hat{S} - \varphi\mathrm{sat}(\hat{S}) - \hat{\Psi}(\cdot)\right] \tag{11}$$

where ζ and φ are control gains which are chosen to fulfill the attractiveness of the estimated sliding surface $\hat{S}$.

Note that POSMC does not require an accurate system model and only one state measurement $y = x_1$ is needed. As the upper bound of perturbation $\Psi(\cdot)$ is replaced by the smaller bound of its estimation error $\tilde{\Psi}(\cdot)$, a smaller control gain is needed such that the over-conservativeness of SMC can be avoided (Jiang, Wu and Wen, 2002).

Remark 2. The motivation to use SMSPO is due to the fact that the sliding-mode observer potentially offers advantages similar to those of sliding-mode controllers, in particular, inherent robustness to parameter uncertainty and external disturbances (Slotine and Li, 1991). It is a high-performance state estimator with a simple structure and is well suited for uncertain nonlinear systems (Kwon and Chung, 2004). Moreover, it has the merits of simple structure and easy analysis of the closed-loop system stability compared to that of ADRC which uses a nonlinear observer (Han, 2009), while they can provide almost the same performance of perturbation estimation.

The overall design procedure of POSMC for system (5) can be summarized as follows:

Step 1: Define perturbation (6) for the original nth-order system (5);

Step 2: Define a *fictitious state* $x_{n+1} = \Psi(\cdot)$ to represent perturbation (6);

Step 3: Extend the original nth-order system (5) into the extended $(n+1)$th-order system (8);

Step 4: Design the $(n+1)$th-order SMSPO (9) for the extended $(n+1)$th-order system (8) to obtain the state estimate $\hat{x}$ and the perturbation estimate $\hat{\Psi}(\cdot)$ by the only measurement of x_1;

Step 5: Design controller (11) for the original nth-order system (5), in which the estimated sliding surface $\hat{S}$ is calculated by (10).

3.2. Rectifier controller design

Choose the system output $y_{\mathrm{r}} = [y_{\mathrm{r1}}, y_{\mathrm{r2}}]^{\mathrm{T}} = [Q_1, V_{\mathrm{dc1}}]^{\mathrm{T}}$, let Q_1^* and V_{dc1}^* be the given references of the reactive power and DC voltage, respectively. Define the tracking error $e_{\mathrm{r}} = [e_{\mathrm{r1}}, e_{\mathrm{r2}}]^{\mathrm{T}} = [Q_1 - Q_1^*, V_{\mathrm{dc1}} - V_{\mathrm{dc1}}^*]^{\mathrm{T}}$, differentiate e_{r} for rectifier (1) until the control input appears explicitly, yields

$$\begin{bmatrix} \dot{e}_{\mathrm{r1}} \\ \ddot{e}_{\mathrm{r2}} \end{bmatrix} = \begin{bmatrix} f_{\mathrm{r1}} - \dot{Q}_1^* \\ f_{\mathrm{r2}} - \ddot{V}_{\mathrm{dc1}}^* \end{bmatrix} + B_{\mathrm{r}} \begin{bmatrix} u_{\mathrm{d1}} \\ u_{\mathrm{q1}} \end{bmatrix} \tag{12}$$

where

$$\begin{cases} f_{\mathrm{r1}} = \dfrac{3u_{\mathrm{sq1}}}{2}\left(-\dfrac{R_1}{L_1}i_{\mathrm{d1}} + \omega i_{\mathrm{q1}}\right) \\ f_{\mathrm{r2}} = \dfrac{3u_{\mathrm{sq1}}}{2C_1V_{\mathrm{dc1}}}\left[-\omega i_{\mathrm{d1}} - \dfrac{R_1}{L_1}i_{\mathrm{q1}} - \dfrac{i_{\mathrm{q1}}}{V_{\mathrm{dc1}}}\left(\dfrac{3u_{\mathrm{sq1}}i_{\mathrm{q1}}}{2C_1V_{\mathrm{dc1}}} - \dfrac{i_{\mathrm{L}}}{C_1}\right)\right] \\ \quad - \dfrac{1}{2R_0C_1}\left(\dfrac{3u_{\mathrm{sq1}}i_{\mathrm{q1}}}{2C_1V_{\mathrm{dc1}}} - \dfrac{i_{\mathrm{L}}}{C_1} - \dfrac{3u_{\mathrm{sq2}}i_{\mathrm{q2}}}{2C_2V_{\mathrm{dc2}}} - \dfrac{i_{\mathrm{L}}}{C_2}\right) \end{cases}$$

and

$$B_{\mathrm{r}} = \begin{bmatrix} \frac{3u_{\mathrm{sq1}}}{2L_1} & 0 \\ 0 & \frac{3u_{\mathrm{sq1}}}{2C_1L_1V_{\mathrm{dc1}}} \end{bmatrix}$$

The determinant of matrix B_{r} is obtained as $|B_{\mathrm{r}}| = 9u_{\mathrm{sq1}}^2/(4C_1L_1^2V_{\mathrm{dc1}})$, which is nonzero within the operation range of the rectifier, thus system (12) is linearizable.

Assume all the nonlinearities are unknown, define the perturbations $\Psi_{\mathrm{r1}}(\cdot)$ and $\Psi_{\mathrm{r2}}(\cdot)$ as

$$\begin{bmatrix} \Psi_{\mathrm{r1}}(\cdot) \\ \Psi_{\mathrm{r2}}(\cdot) \end{bmatrix} = \begin{bmatrix} f_{\mathrm{r1}} \\ f_{\mathrm{r2}} \end{bmatrix} + (B_{\mathrm{r}} - B_{\mathrm{r0}}) \begin{bmatrix} u_{\mathrm{d1}} \\ u_{\mathrm{q1}} \end{bmatrix} \tag{13}$$

where the constant control gain B_{r0} is given by

$$B_{\mathrm{r0}} = \begin{bmatrix} b_{\mathrm{r10}} & 0 \\ 0 & b_{\mathrm{r20}} \end{bmatrix}$$

Then system (12) can be rewritten as

$$\begin{bmatrix} \dot{e}_{\mathrm{r1}} \\ \ddot{e}_{\mathrm{r2}} \end{bmatrix} = \begin{bmatrix} \Psi_{\mathrm{r1}}(\cdot) \\ \Psi_{\mathrm{r2}}(\cdot) \end{bmatrix} + B_{\mathrm{r0}} \begin{bmatrix} u_{\mathrm{d1}} \\ u_{\mathrm{q1}} \end{bmatrix} - \begin{bmatrix} \dot{Q}_1^* \\ \ddot{V}_{\mathrm{dc1}}^* \end{bmatrix} \tag{14}$$

Define $z'_{11} = Q_1$, a second-order sliding-mode perturbation observer (SMPO) is used to estimate $\Psi_{\mathrm{r1}}(\cdot)$ as

$$\begin{cases} \dot{\hat{z}}'_{11} = \hat{\Psi}_{\mathrm{r1}}(\cdot) + \alpha'_{\mathrm{r1}}\tilde{Q}_1 + k'_{\mathrm{r1}}\mathrm{sat}(\tilde{Q}_1) + b_{\mathrm{r10}}u_{\mathrm{d1}} \\ \dot{\hat{\Psi}}_{\mathrm{r1}}(\cdot) = \alpha'_{\mathrm{r2}}\tilde{Q}_1 + k'_{\mathrm{r2}}\mathrm{sat}(\tilde{Q}_1) \end{cases} \tag{15}$$

where observer gains k'_{r1}, k'_{r2}, α'_{r1}, and α'_{r2} are all positive constants.

Define $z_{11} = V_{\rm dc1}$ and $z_{12} = \dot{z}_{11}$, a third-order SMSPO is used to estimate $\Psi_{\rm r2}(\cdot)$ as

$$\begin{cases} \dot{\hat{z}}_{11} = \hat{z}_{12} + \alpha_{\rm r1}\tilde{V}_{\rm dc1} + k_{\rm r1}{\rm sat}(\tilde{V}_{\rm dc1}) \\ \dot{\hat{z}}_{12} = \hat{\Psi}_{\rm r2}(\cdot) + \alpha_{\rm r2}\tilde{V}_{\rm dc1} + k_{\rm r2}{\rm sat}(\tilde{V}_{\rm dc1}) + b_{\rm r20}u_{\rm q1} \\ \dot{\hat{\Psi}}_{\rm r2}(\cdot) = \alpha_{\rm r3}\tilde{V}_{\rm dc1} + k_{\rm r3}{\rm sat}(\tilde{V}_{\rm dc1}) \end{cases} \tag{16}$$

where observer gains $k_{\rm r1}$, $k_{\rm r2}$, $k_{\rm r3}$, $\alpha_{\rm r1}$, $\alpha_{\rm r2}$, and $\alpha_{\rm r3}$ are all positive constants.

The above observers (15) and (16) only need the measurement of reactive power Q_1 and DC voltage $V_{\rm dc1}$ at the rectifier side, which can be directly obtained in practice.

The estimated sliding surface of system (12) is defined as

$$\begin{bmatrix} \hat{S}_{\rm r1} \\ \hat{S}_{\rm r2} \end{bmatrix} = \begin{bmatrix} \hat{z}'_{11} - Q_1^* \\ \rho_1(\hat{z}_{11} - V_{\rm dc1}^*) + \rho_2(\hat{z}_{12} - \dot{V}_{\rm dc1}^*) \end{bmatrix} \tag{17}$$

where ρ_1 and ρ_2 are the positive sliding surface gains. The attractiveness of the estimated sliding surface (17) ensures reactive power Q_1 and DC voltage $V_{\rm dc1}$ can track to their reference.

The POSMC of system (12) is designed as

$$\begin{bmatrix} u_{\rm d1} \\ u_{\rm q1} \end{bmatrix} = B_{\rm r0}^{-1} \begin{bmatrix} -\hat{\Psi}_{\rm r1}(\cdot) + \dot{Q}_1^* - \zeta_{\rm r}'\hat{S}_{\rm r1} - \varphi_{\rm r}'{\rm sat}(\hat{S}_{\rm r1}) \\ -\hat{\Psi}_{\rm r2}(\cdot) + \ddot{V}_{\rm dc1}^* - \zeta_{\rm r}\hat{S}_{\rm r2} - \varphi_{\rm r}{\rm sat}(\hat{S}_{\rm r2}) \end{bmatrix} \tag{18}$$

where positive control gains $\zeta_{\rm r}$, $\zeta_{\rm r}'$, $\varphi_{\rm r}$, and $\varphi_{\rm r}'$ are chosen to ensure the attractiveness of estimated sliding surface (17).

During the most severe disturbance, both the reactive power and DC voltage reduce from their initial value to around zero within a short period of time Δ. Thus the boundary values of the system state and perturbation estimates can be obtained as $|\hat{z}_{11}'| \leq |Q_1^*|$, $|\hat{\Psi}_{\rm r1}(\cdot)| \leq |Q_1^*|/\Delta$, $|\hat{z}_{11}| \leq |V_{\rm dc1}^*|$, $|\hat{z}_{12}| \leq |V_{\rm dc1}^*|/\Delta$, and $|\hat{\Psi}_{\rm r2}(\cdot)| \leq |V_{\rm dc1}^*|/\Delta^2$, respectively.

3.3. Inverter controller design

Choose the system output $y_{\rm i} = [y_{\rm i1}, y_{\rm i2}]^{\rm T} = [Q_2, P_2]^{\rm T}$, let Q_2^* and P_2^* be the given references of the reactive and active power, respectively. Define the tracking error $e_{\rm i} = [e_{\rm i1}, e_{\rm i2}]^{\rm T} = [Q_2 - Q_2^*, P_2 - P_2^*]^{\rm T}$, differentiate $e_{\rm i}$ for inverter (2) until the control input appears explicitly, yields

$$\begin{bmatrix} \dot{e}_{\rm i1} \\ \dot{e}_{\rm i2} \end{bmatrix} = \begin{bmatrix} f_{\rm i1} - \dot{Q}_2^* \\ f_{\rm i2} - \dot{P}_2^* \end{bmatrix} + B_{\rm i} \begin{bmatrix} u_{\rm d2} \\ u_{\rm q2} \end{bmatrix} \tag{19}$$

where

$$\begin{cases} f_{\mathrm{i}1} = \dfrac{3u_{\mathrm{sq}2}}{2}\left(-\dfrac{R_2}{L_2}i_{\mathrm{d}2} + \omega i_{\mathrm{q}2}\right) \\ f_{\mathrm{i}2} = \dfrac{3u_{\mathrm{sq}2}}{2}\left(-\dfrac{R_2}{L_2}i_{\mathrm{q}2} - \omega i_{\mathrm{d}2}\right) \end{cases}$$

and

$$B_{\mathrm{i}} = \begin{bmatrix} \frac{3u_{\mathrm{sq}2}}{2L_2} & 0 \\ 0 & \frac{3u_{\mathrm{sq}2}}{2L_2} \end{bmatrix}$$

The determinant of matrix B_{i} is obtained as $|B_{\mathrm{i}}| = 9u_{\mathrm{s}2}^2/(4L_2^2)$, which is nonzero within the operation range of the inverter, thus system (19) is linearizable.

Assume all the nonlinearities are unknown, define the perturbations $\Psi_{\mathrm{i}1}(\cdot)$ and $\Psi_{\mathrm{i}2}(\cdot)$ as

$$\begin{bmatrix} \Psi_{\mathrm{i}1}(\cdot) \\ \Psi_{\mathrm{i}2}(\cdot) \end{bmatrix} = \begin{bmatrix} f_{\mathrm{i}1} \\ f_{\mathrm{i}2} \end{bmatrix} + (B_{\mathrm{i}} - B_{\mathrm{i}0}) \begin{bmatrix} u_{\mathrm{d}2} \\ u_{\mathrm{q}2} \end{bmatrix} \tag{20}$$

where the constant control gain $B_{\mathrm{i}0}$ is given by

$$B_{\mathrm{i}0} = \begin{bmatrix} b_{\mathrm{i}10} & 0 \\ 0 & b_{\mathrm{i}20} \end{bmatrix}$$

Then system (19) can be rewritten as

$$\begin{bmatrix} \dot{e}_{\mathrm{i}1} \\ \dot{e}_{\mathrm{i}2} \end{bmatrix} = \begin{bmatrix} \Psi_{\mathrm{i}1}(\cdot) \\ \Psi_{\mathrm{i}2}(\cdot) \end{bmatrix} + B_{\mathrm{i}0} \begin{bmatrix} u_{\mathrm{d}2} \\ u_{\mathrm{q}2} \end{bmatrix} - \begin{bmatrix} \dot{Q}_2^* \\ \dot{P}_2^* \end{bmatrix} \tag{21}$$

Similarly, define $z'_{21} = Q_2$ and $z_{21} = P_2$, two second-order SMPOs are used to estimate $\Psi_{\mathrm{i}1}(\cdot)$ and $\Psi_{\mathrm{i}2}(\cdot)$, respectively, as

$$\begin{cases} \dot{\hat{z}}'_{21} = \hat{\Psi}_{\mathrm{i}1}(\cdot) + \alpha'_{\mathrm{i}1}\tilde{Q}_2 + k'_{\mathrm{i}1}\mathrm{sat}(\tilde{Q}_2) + b_{\mathrm{i}10}u_{\mathrm{d}2} \\ \dot{\hat{\Psi}}_{\mathrm{i}1}(\cdot) = \alpha'_{\mathrm{i}2}\tilde{Q}_2 + k'_{\mathrm{i}2}\mathrm{sat}(\tilde{Q}_2) \end{cases} \tag{22}$$

where observer gains $k'_{\mathrm{i}1}$, $k'_{\mathrm{i}2}$, $\alpha'_{\mathrm{i}1}$, and $\alpha'_{\mathrm{i}2}$ are all positive constants.

$$\begin{cases} \dot{\hat{z}}_{21} = \hat{\Psi}_{\mathrm{i}2}(\cdot) + \alpha_{\mathrm{i}1}\tilde{P}_2 + k_{\mathrm{i}1}\mathrm{sat}(\tilde{P}_2) + b_{\mathrm{i}20}u_{\mathrm{q}2} \\ \dot{\hat{\Psi}}_{\mathrm{i}2}(\cdot) = \alpha_{\mathrm{i}2}\tilde{P}_2 + k_{\mathrm{i}2}\mathrm{sat}(\tilde{P}_2) \end{cases} \tag{23}$$

where observer gains $k_{\mathrm{i}1}$, $k_{\mathrm{i}2}$, $\alpha_{\mathrm{i}1}$, and $\alpha_{\mathrm{i}2}$ are all positive constants .

The above observers (22) and (23) only need the measurement of reactive power Q_2 and active power P_2 at the inverter side, which can be directly obtained in practice.

The estimated sliding surface of system (19) is defined as

$$\begin{bmatrix} \hat{S}_{\mathrm{i1}} \\ \hat{S}_{\mathrm{i2}} \end{bmatrix} = \begin{bmatrix} \hat{z}_{21}' - Q_2^* \\ \hat{z}_{21} - P_2^* \end{bmatrix} \tag{24}$$

Similarly, the attractiveness of the estimated sliding surface (24) ensures the reactive power Q_2 and active power P_2 can track to their reference.

The POSMC of system (19) is designed as

$$\begin{bmatrix} u_{\mathrm{d2}} \\ u_{\mathrm{q2}} \end{bmatrix} = B_{\mathrm{i0}}^{-1} \begin{bmatrix} -\hat{\Psi}_{\mathrm{i1}}(\cdot) + \dot{Q}_2^* - \zeta_{\mathrm{i}}' \hat{S}_{\mathrm{i1}} - \varphi_{\mathrm{i}}' \mathrm{sat}(\hat{S}_{\mathrm{i1}}) \\ -\hat{\Psi}_{\mathrm{i2}}(\cdot) + \dot{P}_2^* - \zeta_{\mathrm{i}} \hat{S}_{\mathrm{i2}} - \varphi_{\mathrm{i}} \mathrm{sat}(\hat{S}_{\mathrm{i2}}) \end{bmatrix} \tag{25}$$

where positive control gains ζ_{i}, ζ_{i}, φ_{i}, and φ_{i}' are chosen to ensure the attractiveness of estimated sliding surface (24).

Similarly, the boundary values of the system state and perturbation estimates can be obtained as $|\hat{z}_{21}'| \le |Q_2^*|$, $|\hat{\Psi}_{\mathrm{i1}}(\cdot)| \le |Q_2^*|/\Delta$, $|\hat{z}_{21}| \le |P_2^*|$, and $|\hat{\Psi}_{\mathrm{i2}}(\cdot)| \le |P_2^*|/\Delta$, respectively.

Note that control outputs (18) and (25) are modulated by the sinusoidal pulse width modulation (SPWM) technique (Nikolas, Vassilios, and Georgios, 2009) in this paper. The overall controller structure of the VSC-HVDC system is illustrated by Fig. 2, in which only reactive power Q_1 and DC

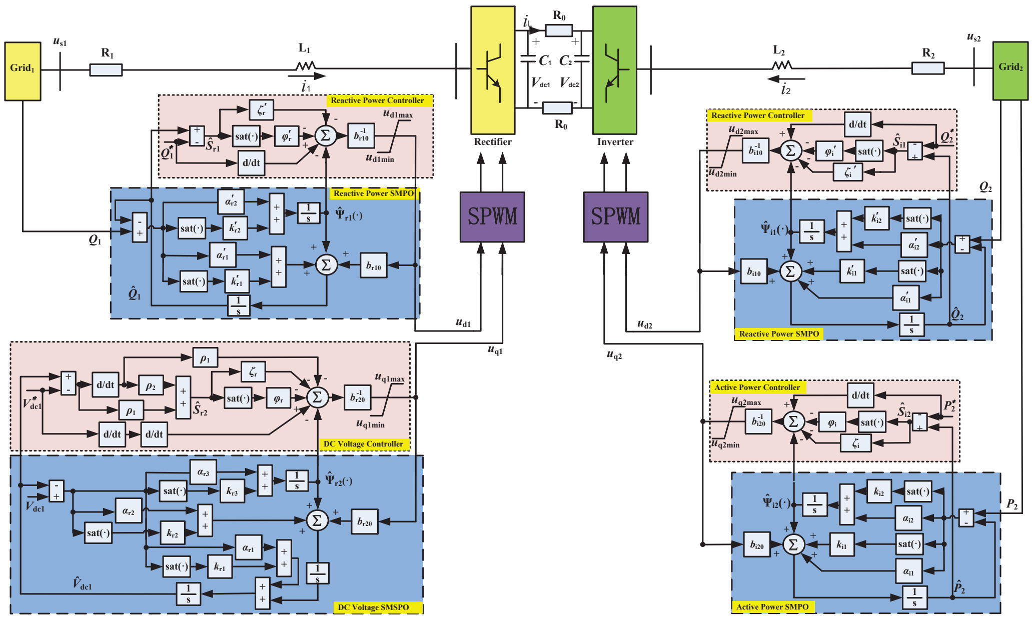

Figure 2: The overall controller structure of the VSC-HVDC system.

voltage V_{dc1} need to be measured for rectifier controller (18), while active power P_2 and reactive power Q_2 for inverter controller (25).

4. Simulation Results

POSMC is applied on the VSC-HVDC system illustrated in Fig. 1. The AC grid frequency is 50 Hz and VSC-HVDC system parameters are given in Table 1. POSMC parameters are provided in Table 2, in which the observer poles are allocated as $\lambda_{\alpha_{\mathrm{r}}} = 100$ and $\lambda_{\alpha'_{\mathrm{r}}} = \lambda_{\alpha_{\mathrm{i}}} = \lambda_{\alpha'_{\mathrm{i}}} = 20$, while control inputs are bounded as $|u_{\mathrm{q}i}| \leq 80$ kV and $|u_{\mathrm{d}i}| \leq 60$ kV, where $i = 1, 2$. The

Table 1: The VSC-HVDC system parameters

AC system based voltage	$V_{\mathrm{AC_{base}}}$	132 kV
DC cable base voltage	$V_{\mathrm{DC_{base}}}$	150 kV
System base power	S_{base}	100 MVA
AC system resistance (25 km)	R_1, R_2	0.05 Ω/km
AC system inductance (25 km)	L_1, L_2	0.026 mH/km
DC cable resistance (50 km)	R_0	0.21 Ω/km
DC bus capacitance	C_1, C_2	11.94 μF

switching frequency is 1620 Hz for both rectifier and inverter, which is taken from (Moharana and Dash, 2010). The control performance of POSMC is compared to that of VC (Li, Haskew and Xu, 2010) and FLSMC (Moharana and Dash, 2010) by the following four cases.

Table 2: POSMC parameters for the VSC-HVDC system

Rectifier controller gains			
$b_{\mathrm{r}10} = 100$	$b_{\mathrm{r}20} = 7000$	$\rho_1 = 800$	$\rho_2 = 1$
$\zeta_{\mathrm{r}} = 20$	$\zeta'_{\mathrm{r}} = 10$	$\varphi_{\mathrm{r}} = 20$	$\varphi'_{\mathrm{r}} = 20$
Rectifier observer gains			
$\alpha_{\mathrm{r}1} = 300$	$\alpha'_{\mathrm{r}1} = 40$	$\alpha_{\mathrm{r}2} = 3 \times 10^4$	$\alpha'_{\mathrm{r}2} = 400$
$\alpha_{\mathrm{r}3} = 10^6$	$\Delta = 0.01$	$\epsilon = 0.1$	$k_{\mathrm{r}1} = 100$
$k'_{\mathrm{r}1} = 75$	$k_{\mathrm{r}2} = 10^5$	$k'_{\mathrm{r}2} = 3.75 \times 10^4$	$k_{\mathrm{r}3} = 2.5 \times 10^7$
Inverter controller gains			
$b_{\mathrm{i}10} = 50$	$b_{\mathrm{i}20} = 50$	$\zeta_{\mathrm{i}} = 10$	$\zeta'_{\mathrm{i}} = 10$
$\varphi_{\mathrm{i}} = 10$	$\varphi'_{\mathrm{i}} = 10$		
Inverter observer gains			
$\alpha_{\mathrm{i}1} = 40$	$\alpha'_{\mathrm{i}1} = 40$	$\alpha_{\mathrm{i}2} = 400$	$\alpha'_{\mathrm{i}2} = 400$
$k_{\mathrm{i}1} = 75$	$k'_{\mathrm{i}1} = 75$	$k_{\mathrm{i}2} = 3.75 \times 10^4$	$k'_{\mathrm{i}2} = 3.75 \times 10^4$

1) Case 1: Active and reactive power tracking: The references of active and reactive power are set to be a series of step change occurs at $t = 0.2$ s,

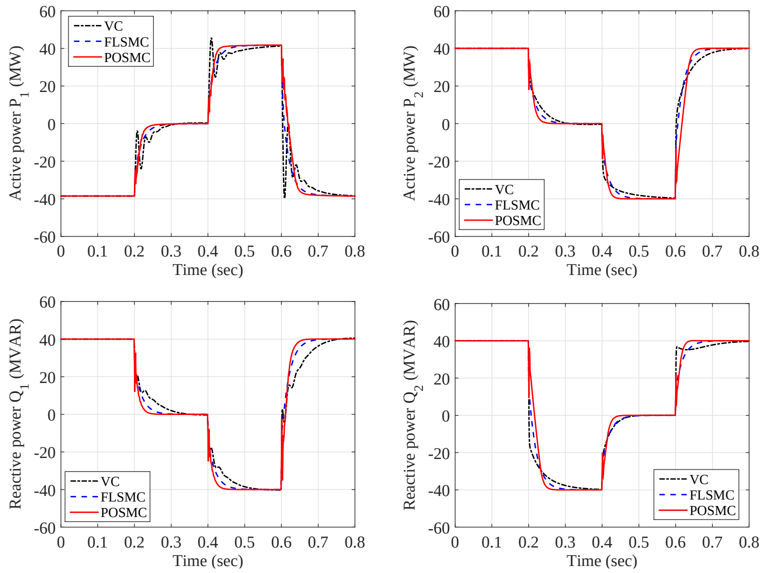

Figure 3: System responses obtained under the active and reactive power tracking.

$t = 0.4$ s, and restores to the original value at $t = 0.6$ s, while DC voltage is regulated at the rated value $V_{\mathrm{dc1}}^{*} = 150$ kV. The system responses are illustrated by Fig. 3. One can find that POSMC has the fastest tracking rate and maintains a consistent control performance under different operation conditions.

2) Case 2: 5-cycle line-line-line-ground (LLLG) fault at AC bus 1. A 5-cycle LLLG fault occurs at AC bus 1 when $t = 0.1$ s. Due to the fault, AC voltage at the corresponding bus is decreased to a critical level. Fig. 4 shows that POSMC can effectively restore the system with smallest active power oscillations. Response of perturbation estimation is demonstrated in Fig. 5,

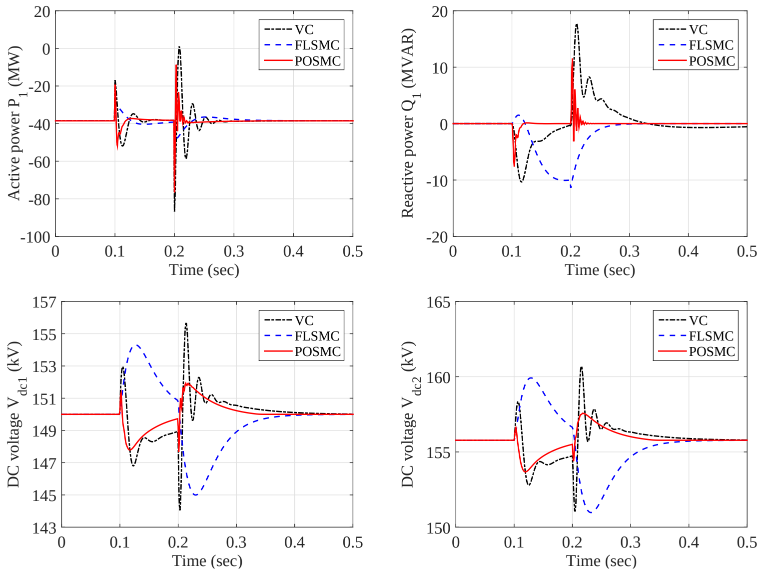

Figure 4: System responses obtained under the 5-cycle LLLG fault at AC bus 1.

which shows SMSPO and SMPO can estimate the perturbations with a fast tracking rate.

3) Case 3: Weak AC grid connection: The AC grids are assumed to be sufficiently strong such that AC bus voltages are ideal constants. It is worth

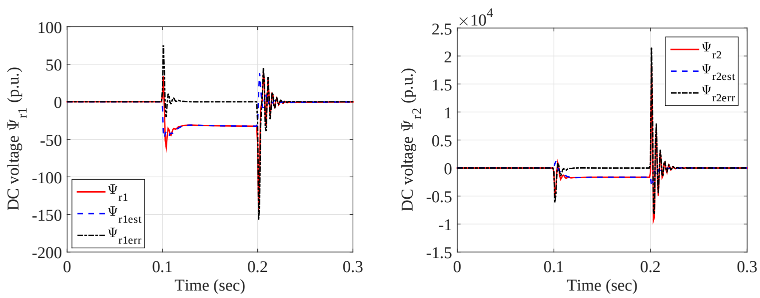

Figure 5: Estimation errors of the perturbations obtained under the 5-cycle LLLG fault at AC bus 1.

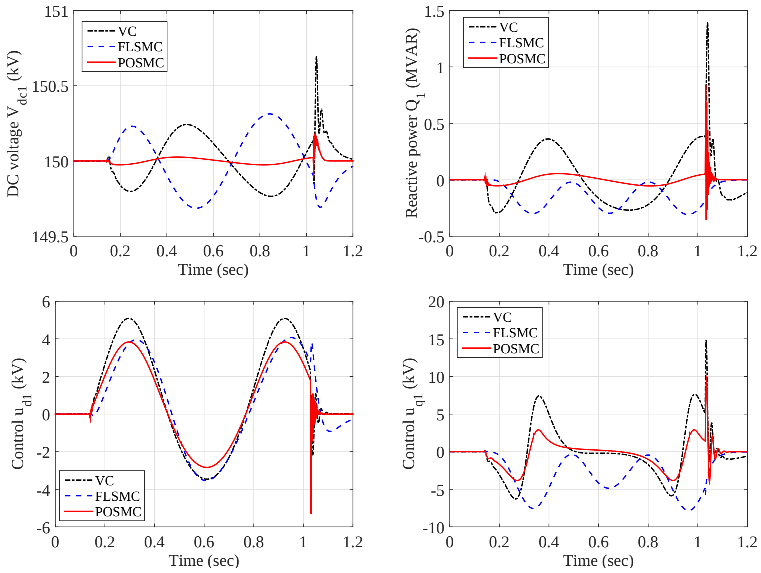

Figure 6: System responses obtained with the weak AC grid connection.

considering a weak AC grid connected to the rectifier, e.g., offshore wind farms, which voltage u_{s1} is no longer a constant but a time-varying function. A voltage fluctuation occurs from 0.15 s to 1.05 s caused by the wind speed variation is applied, which corresponds to $u_{s1} = 1 + 0.15 \sin(0.2\pi t)$. System responses are presented in Fig. 6, it illustrates that both DC voltage and reactive power are oscillatory, while POSMC can effectively suppress such oscillation with the smallest fluctuation of DC voltage and reactive power.

4) Case 4: System parameter uncertainties: When there is a fault in the transmission or distribution grid, the resistance and inductance values of the grid may change significantly. Several tests are performed for plant-model

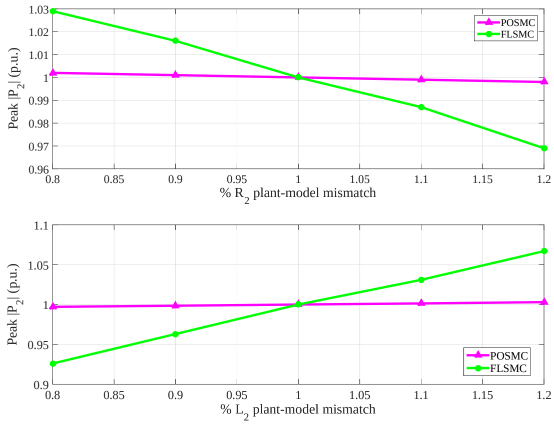

Figure 7: The peak active power $|P_2|$ (in p.u.) to a -120 A in the DC cable current i_{L} obtained at nominal grid voltage for plant-model mismatches in the range of 20% (one parameter changes and others keep constant).

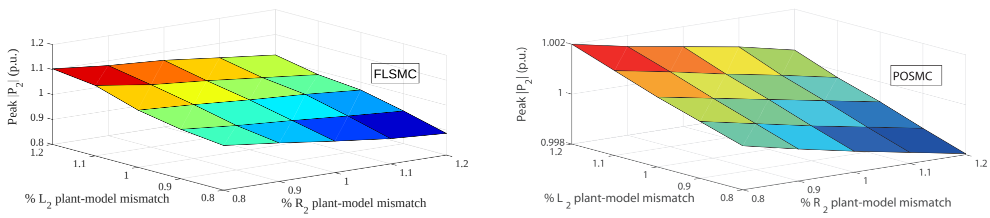

Figure 8: The peak active power $|P_2|$ (in p.u.) to a -120 A in the DC cable current i_{L} obtained at nominal grid voltage for plant-model mismatches in the range of 20% (different parameters may change at the same time).

mismatches of R_2 and L_2 with $\pm 20\%$ uncertainties. All tests are undertaken under the nominal grid voltage and a corresponding -120 A in the DC cable current i_{L} at 0.1 s. The peak active power $|P_2|$ is recorded which uses per unit (p.u.) value for a clear illustration of system robustness. It can be found from Fig. 7 that the peak active power $|P_2|$ controlled by POSMC is almost not affected, while FLSMC has a relatively large range of variation, i.e., around 3% to R_2 and 8% to L_2, respectively. Responses to mismatch of R_2 and L_2 changing at the same time are demonstrated in Fig. 8. The magnitude of changes is around 10% under FLSMC and almost does not change under POSMC. This is because POSMC estimates all uncertainties and does not need an accurate system model, thus it has better robustness than that of FLSMC which requires accurate system parameters.

The integral of absolute error (IAE) indices of each approach calculated in different cases are tabulated in Table 3. Here $\mathrm{IAE}_{Q_1} = \int_0^T |Q_1 - Q_1^*|\mathrm{d}t$, $\mathrm{IAE}_{V_{\mathrm{dc1}}} = \int_0^T |V_{\mathrm{dc1}} - V_{\mathrm{dc1}}^*|\mathrm{d}t$, $\mathrm{IAE}_{Q_2} = \int_0^T |Q_2 - Q_2^*|\mathrm{d}t$ and $\mathrm{IAE}_{P_2} = \int_0^T |P_2 - P_2^*|\mathrm{d}t$. The simulation time T=3 s. Note that POSMC has a little bit higher IAE than that of FLSMC in the power tracking due to the estimation error, while it can provide much better robustness in the case of 5-cycle LLLG fault and weak AC grid connection. In particular, its IAE_{Q_1} and $\mathrm{IAE}_{V_{\mathrm{dc1}}}$ are only

Table 3: IAE indices (in p.u.) of different control schemes calculated in different cases

Case / Method	Power tracking			
	$\mathrm{IAE_{Q_1}}$	$\mathrm{IAE_{V_{dc1}}}$	$\mathrm{IAE_{Q_2}}$	$\mathrm{IAE_{P_2}}$
VC	3.83E-02	4.44E-03	2.13E-02	2.71E-02
FLSMC	2.19E-02	1.73E-03	2.23E-02	2.18E-02
POSMC	2.33E-02	2.00E-03	2.42E-02	2.33E-02
Case / Method	**5-cycle LLLG fault**		**Weak AC grid connection**	
	$\mathrm{IAE_{Q_1}}$	$\mathrm{IAE_{V_{dc1}}}$	$\mathrm{IAE_{Q_1}}$	$\mathrm{IAE_{V_{dc1}}}$
VC	2.62E-02	2.15E-03	4.53E-03	4.13E-03
FLSMC	1.13E-02	4.13E-03	4.08E-03	3.33E-03
POSMC	5.64E-03	1.38E-03	3.88E-04	6.78E-04

8.57% and 9.51% of those of VC, 16.42% and 20.36% of those of FLSMC with the weak AC grid connection. The overall control costs are illustrated in Fig. 9, with $\mathrm{IAE}_u = \int_0^T (|u_{\mathrm{d1}}| + |u_{\mathrm{q1}}| + |u_{\mathrm{d2}}| + |u_{\mathrm{q2}}|)\mathrm{d}t$. It is obvious that POSMC has the lowest control costs in all cases, which is resulted from the merits that the upper bound of perturbation is replaced by the smaller bound of its estimation error, thus an over-conservative control input can be avoided.

5. Hardware-in-the-loop Test Results

A dSPACE simulator based HIL test is used to validate the implementation feasibility of POSMC, which configuration and experiment platform are given by Fig. 10 and Fig. 11, respectively. The rectifier controller (18) and

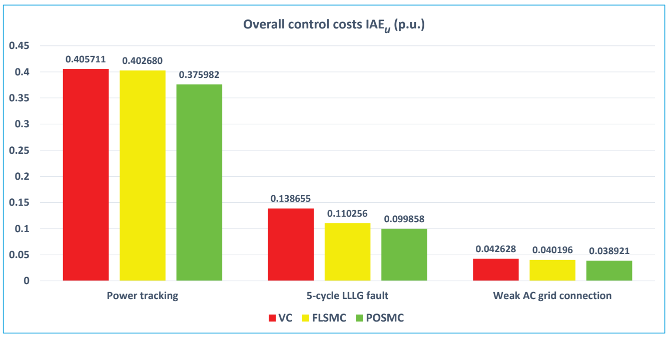

Figure 9: Overall control costs $\mathrm{IAE_u}$ (in p.u.) obtained in different cases

inverter controller (25) are implemented on one dSPACE platform (DS1104 board) with a sampling frequency $f_\mathrm{c} = 1$ kHz, and the VSC-HVDC system is simulated on another dSPACE platform (DS1006 board) with the limit sampling frequency $f_\mathrm{s} = 50$ kHz to make HIL simulator as close to the real plant as possible. The measurements of the reactive power Q_1, DC voltage $V_{\mathrm{dc}1}$, active power P_2 and reactive power Q_2 are obtained from the real-time simulation of the VSC-HVDC system on the DS1006 board, which are sent to two controllers implemented on the DS1104 board for the control inputs calculation.

It follows from (Yang, Jiang, Yao and Wu, 2015) that an unexpected high-frequency oscillation in control inputs may emerge as the large observer poles would result in high gains, which lead to highly sensitive observer dynamics to the measurement disturbances in the HIL test . Note that this phenomenon

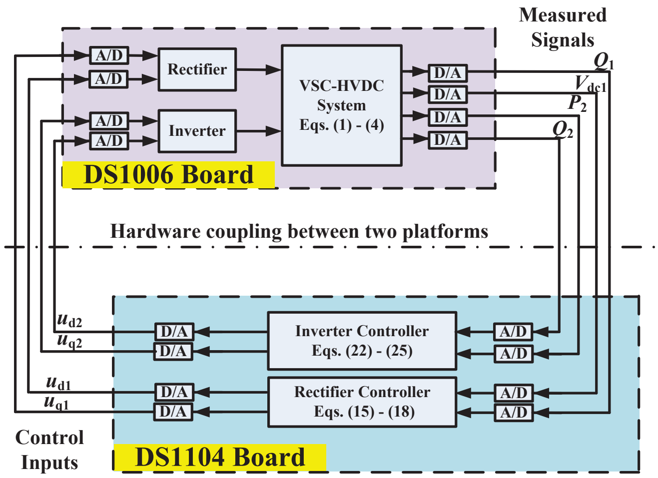

Figure 10: The configuration of the HIL test.

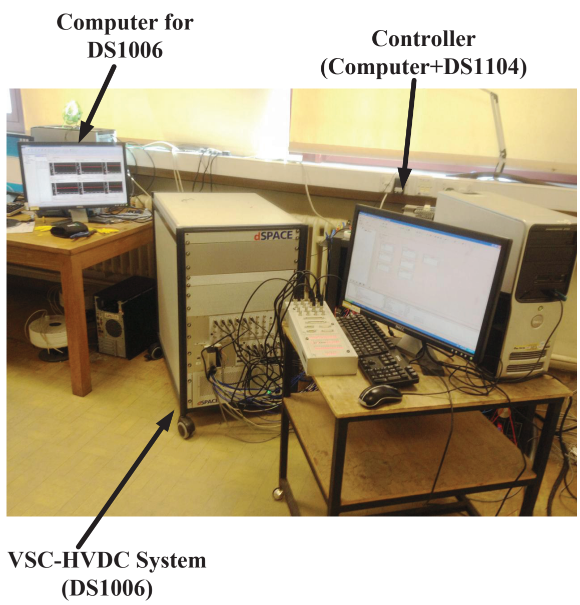

Figure 11: The experiment platform of the HIL test.

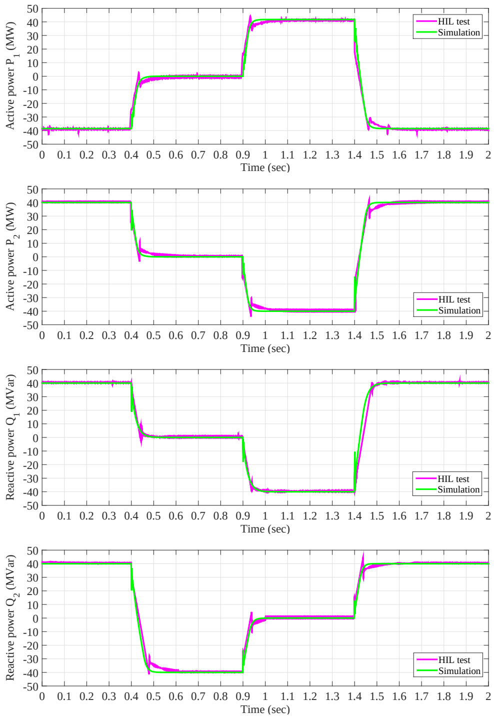

Figure 12: HIL test results of system responses obtained under the active and reactive power tracking.

does not exist in the simulation. One effective way to alleviate such malignant effect is to reduce the observer poles. Through trial-and-error, an observer pole in the range of $\lambda_{\alpha_{\mathrm{r}}} \in [15, 25]$ and $\lambda_{\alpha'_{\mathrm{r}}} = \lambda_{\alpha_{\mathrm{i}}} = \lambda_{\alpha'_{\mathrm{i}}} \in [3, 10]$ can avoid such oscillation but with almost similar transient responses, thus the reduced poles $\lambda_{\alpha_{\mathrm{r}}} = 20$ and $\lambda_{\alpha'_{\mathrm{r}}} = \lambda_{\alpha_{\mathrm{i}}} = \lambda_{\alpha'_{\mathrm{i}}} = 5$, with $b_{\mathrm{r}10} = 50$, $b_{\mathrm{r}20} = 5000$, $b_{\mathrm{i}10} = 20$, and $b_{\mathrm{i}20} = 20$, are chosen in the HIL test. Furthermore, a time delay $\tau = 3$ ms has been assumed in the corresponding simulation to consider the effect of the computational delay of the real-time controller.

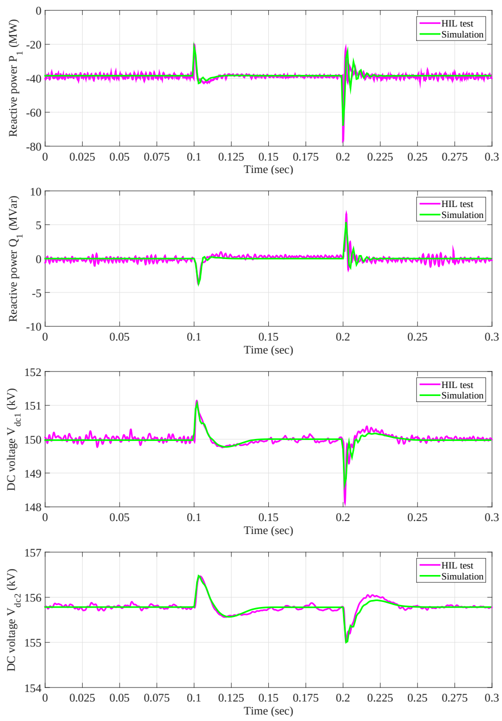

Figure 13: HIL test results of system responses obtained under the 5-cycle LLLG fault at AC bus 1.

1) Case 1: Active and reactive power tracking: The reference of active and reactive power changes at $t = 0.4$ s, $t = 0.9$ s, and restores to the original value at $t = 1.4$ s, while DC voltage is regulated at the rated value $V^*_{\mathrm{dc1}} = 150$ kV. The system responses obtained under the HIL test and simulation are compared by Fig. 12, which shows that the HIL test has almost the same results as that of the simulation.

2) Case 2: 5-cycle line-line-line-ground (LLLG) fault at AC bus 1. A 5-cycle LLLG fault occurs at AC bus 1 when $t = 0.1$ s. Fig. 13 demonstrates

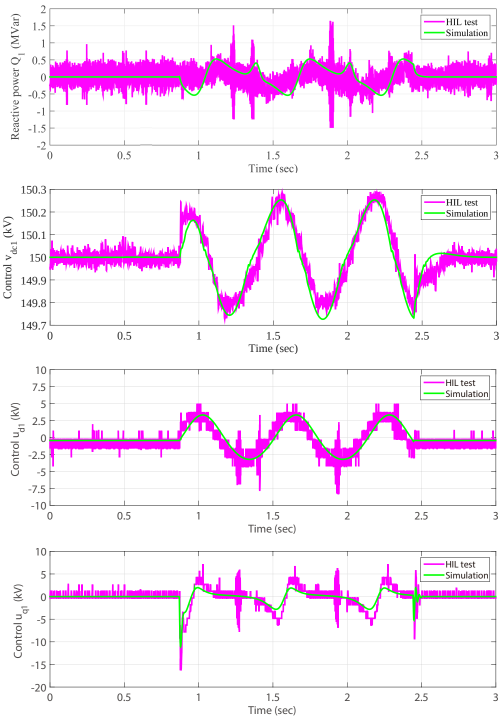

Figure 14: HIL test results of system responses obtained with the weak AC grid connection.

that the system can be rapidly restored and the system responses obtained by the HIL test is similar to that of simulation.

3) Case 3: Weak AC grid connection: The same voltage variation $u_{s1} = 1 + 0.15\sin(0.2\pi t)$ is applied between 0.87 s to 2.45 s. It can be readily seen from Fig. 14 that the results of the HIL test and simulation match very well.

The difference of the obtained results between the HIL test and simulation is possibly due to the following two reasons:

- There exist measurement disturbances in the HIL test which are however not taken into account in the simulation, a filter could be used to remove the measurement disturbances thus the control performance can be improved.

- The sampling frequency of VSC-HVDC model and POSMC is the same in simulation (f_s=f_c=1 kHz) as they are implemented in Matlab of the same computer. In contrast, the sampling frequency of VSC-HVDC model (f_s=50 kHz) is significantly increased in the HIL test to make VSC-HVDC model as close to the real plant as possible. Note the sampling frequency of POSMC remains the same (f_c=1 kHz) due to the sampling limit of the practical controller.

6. Conclusion

A POSMC scheme has been developed for the VSC-HVDC system to rapidly compensate the combinatorial effect of nonlinearities, parameter uncertainties, unmodelled dynamics and time-varying external disturbances. As the upper bound of perturbation is replaced by the smaller bound of its estimation error, an over-conservative control input is avoided such that the tracking accuracy can be improved.

Four case studies have been undertaken to evaluate the control performance of the proposed approach, which verify that POSMC can maintain a consistent control performance with less power overshoot during the power reversal, restore the system rapidly after the AC fault, suppress the oscillation effectively when connected to a weak AC grid, and provide significant robustness in the presence of system parameter uncertainties. At last, an HIL test has been carried out which validates the implementation feasibility of POSMC.

Acknowledgements

This work is supported by the China Scholarship Council (CSC), and also supported in part by National key research program of China(973 program)(2014CB247400) and in part by National Natural Science Foundation of China under Grant No. 51428702.

Beltran B., Ahmed-Ali T., and Benbouzid M. E. H., (2008) Sliding mode power control of variable-speed wind energy conversion systems, *IEEE Transactions on Industrial Electronics*, 3314-3321.

Chen W. H., Ballance D. J., Gawthrop P. J., and O'Reilly J., (2000) A nonlinear disturbance observer for robotic manipulators, *IEEE Transactions on Industrial Electronics*, *27*(4), 932-938.

Durrant M., Werner H., and Abbott K., (2004) Synthesis of multi-objective controllers for a VSC HVDC terminal using LMIs, in *IEEE Conference of Decision and Control*, 4473-4478.

Edwards C. and Spurgeon S., (1998) Sliding mode control: theory and applications, CRC Press.

Flourentzou N., Agelidis V. G., and Demetriades G. D., (2009). VSC-based HVDC power transmission systems: an overview, *IEEE Transactions on Power Electronics*, *24*(3), 592-602.

Gokasan M., Bogosyan S., and Goering D. J., (2006) Sliding mode based powertrain control for efficiency improvement in series hybrid-electric vehicles, *IEEE Transactions on Power Electronics*, *21*(3), 779-790.

Guo B. Z. and Zhao Z. L., (2011) On the convergence of an extended state observer for nonlinear systems with uncertainty, *Systems & Control Letters*, *60*(6), 420-430.

Haileselassie T. M., Molinas M., and Undeland T., (2008) Multi-terminal VSCHVDC system for integration of offshore wind farms and green electrification of platforms in the North Sea, *presented at the Nordic Workshop on Power and Industrial Electronics*, Otakaari, Finland.

Han J. Q., (2009) From PID to active disturbance rejection control, *IEEE Transactions on Industrial Electronics*, *56*, 900-906.

Hernandez J. and Barbot J. P., (1996) Sliding observer-based feedback control for flexible joints manipulator. *Automatica*, *32*(9), 1243-1254.

Hertema D. V. and Ghandhari M., (2010). Multi-terminal VSC HVDC for the European supergrid: Obstacles, *Renewable and Sustainable Energy Reviews*, *14*, 3156-3163.

Huo W., (2008) Predictive variable structure control of nonholonomic chained systems, *International Journal of Computer Mathematics-Computer Mathematics in Dynamics and Control*, *85*(6), 949-960.

Jiang L.(2001) Nonlinear adaptive control and applications in power systems, *PhD Thesis, University of Liverpool*.

Jiang L., Wu Q. H., and Wen J. Y., (2002) Nonlinear adaptive control via sliding-mode state and perturbation observer, *IEE Proc. Control Theory and Applications*, *149*(4), 269-277.

Johnson C., (1971) Accommodation of external disturbances in linear regulator and servomechanism problems, *IEEE Transactions on Automatic Control*, *16*(6), 635-644.

Jovcic D., (2003) Phase locked loop system for FACTS, *IEEE Transactions on Power Systems*, *18*(3), 1116-1124.

Kessal A. and Rahmani L., (2014) Ga-optimized parameters of sliding-mode controller based on both output voltage and input current with an application in the PFC of AC/DC converters, *IEEE Transactions on Power Electronics*, *29*(6), 3159-3165.

Kwon S. J. and Chung W. K., (2004) Perturbation compensator based robust tracking control and state estimation of mechanical systems. Springer, New York.

Lascu C., Boldea I., and Blaabjerg F., (2004) Direct torque control of sensorless induction motor dirves: A sliding-mode approach, *IEEE Transactions on Industrial Electronics*, *40*(2), 582-590.

Li S., Haskew T. A., and Xu L., (2010) Control of HVDC light system using conventional and direct current vector control approaches, *IEEE Transactions on Power Electronics*, *25*(12), 3106-3118.

Liu Y., Wu Q. H., Zhou X. X., and Jiang L., (2014) Perturbation observer based multiloop control for the DFIGWT in multimachine power system. *IEEE Transactions on Power Systems*, *29*(6),2905-2915.

Lordelo A. and Fazzolari H., (2014) On interval goal programming switching surface robust design for integral sliding mode control, *Control Engineering Practice*, *32*, 136-146.

Moharana A. and Dash P. K., (2010) Input-output linearization and robust sliding-mode controller for the VSC-HVDC transmission link, *IEEE Transactions on Power Delivery*, *25*(3), 1952-1961.

Nikolas F., Vassilios G. A., and Georgios D. D., (2009) VSC-based HVDC power transmission systems: An overview, *IEEE Transactions on Power Electronics*, *24*(3), 592-602.

Ruan S. Y., Li G. J., Jiao X. H., Sun Y. Z., and Lie T., (2007) Adaptive control design for VSC-HVDC systems based on backstepping method, *Electric Power Systems Research*, *77*, 559-565.

Ruan S. Y., Li G. J., Peng L., Sun Y. Z., and Lie T. T., (2007) A nonlinear control for enhancing HVDC light transmission system stability, *International Journal of Electric Power and Energy Systems*, *27*, 565-570.

Slotine, J.J.E. and Li, W., (1991) Applied nonlinear control. *Prentice-Hall, London.*

Sanchis R. and Nijmeijer H., (1998) Sliding controller-sliding observer design for nonlinear systems. *European Journal of Control*, *4*, 208-234.

She J. H., Fang M., Ohyama Y., Hashimoto H., and Wu M., (2008) Improving disturbance-rejection performance based on an equivalent-inputdisturbance approach, *IEEE Transactions on Industrial Electronics*, *55*(1), 380-389.

Sun L., Li D. H., and Lee K. Y., (2015) Enhanced decentralized PI control for fluidized bed combustor via advanced disturbance observer, *Control Engineering Practice*, *42*, 128-139.

Sun L., Dong J. Y., Li D. H., and Lee K. Y., (2016) A practical multi-variable control approach based on inverted decoupling and decentralized active disturbance rejection control. *Industrial & Engineering Chemistry Research*, *55*(7), 2008-2019.

Wang J. X., Li S. H., Yang J., Wu B. and Li Q., (2015) Extended state observer-based sliding mode control for PWM-based DC-DC buck power converter systems with mismatched disturbances," *IET Control Theory and Applications*, *9*(4), 579-586.

Xia Y., Zhu Z., and Fu M., (2011) Back-stepping sliding mode control for missile systems based on an extended state observer, *IET Control Theory and Applications*, *5*(1), 93-102.

Yang B., Jiang L., Yao W., and Wu Q. H., (2015) Perturbation estimation based coordinated adaptive passive control for multimachine power systems. *Control Engineering Practice*, *44*, 172-192.

Yue M., Liu B. Y., An C., and Sun X. J., (2014) Extended state observer-based adaptive hierarchical sliding mode control for longitudinal movement of a spherical robot, *Nonlinear Dynamics*, *78*, 1233-1244.

Zhang L., Harnefors L., and Nee H.P., (2011) Interconnection of two very weak AC systems by VSC-HVDC links using power-synchronization control, *IEEE Transactions on Power Systems*, *26*(1), 344-355.

Zhang L., Harnefors L. and Nee H. P., (2011) Modeling and control of VSC-HVDC links connected to island systems, *IEEE Transactions on Power Systems*, *26*(2), 783-793.

Zong Q., Zhao Z. S., and Zhang J., (2010) Higher order sliding mode control with self-tuning law based on integral sliding mode, *IET Control Theory and Applications*, *4* (7), 1282-1289.